Flame-splitting mechanism of buoyancy-controlled diffusion plumes generated by a rectangular fire source attached to a sidewall

Xianjia Huang[a], Jinkai Wang[b], He Zhu[b], Chaoliang Xing[a], Jennifer Wen [c], Fei Tang[d, *]

[a] Joint Laboratory of Nuclear Power Plant Fire Safety, Institute of Industrial Technology Guangzhou, Guangzhou 511458, China

[b] State Key Laboratory of Nuclear Power Monitoring Technology and Equipment, China Nuclear Power Design Co., Ltd., Shenzhen 518045, China

[c] School of Engineering, University of Warwick, Coventry CV4 7AL, UK

[d] State Key Laboratory of Fire Science, University of Science and Technology of China, Hefei, Anhui 230026, China

*Corresponding author:

Email address: ftang@ustc.edu.cn;

Postal address: State Key Laboratory of Fire Science, University of Science and Technology of China, Hefei, Anhui 230026, China

Abstract

Flame morphology is an important characteristic parameter for buoyant-controlled fuel diffusion flames. In this study, fire tests were conducted using rectangular burners placed against a thermally thin sidewall. Measurements were obtained for the flame morphology and temperature distribution on the back side of the sidewall. When the aspect ratio of the fire source was 7.45, flame branching into two regions was observed and was further evidenced by the temperature distributions on the corresponding two heated regions on the sidewall. The mechanism of the flame split was investigated, and numerical simulations and physical analyses were performed. The flame split occurred when the entrained air from the middle of the burner length was not consumed before it reached the bottom of the sidewall. Therefore, an appropriate ratio of flame height to burner length was proposed for the occurrence of the flame split. The critical ratio for the flame split was validated by other fire experiments of fire sources located against the sidewall.

Keywords:

Rectangular fuel fire; Flame split; Thermally thin sidewall; Flame morphology; Back-side temperature.

1. Introduction

Buoyant turbulent diffusion flame morphology, including rectangular fire plumes, is an important characteristic parameter. Rectangular flame characteristics have attracted significant research attention. The characteristics of the flame height [1–6], spatial temperature and velocity distribution [1, 2, 7, 8], and thermal radiation [9] produced by a rectangular fire source in a normal atmosphere have been studied experimentally. The effect of sub-atmospheric pressure on the characteristics of a rectangular fire source has also been investigated [10–15].

The sidewall effect has a considerable influence on the flame characteristics of nearby fires [16–21]. Fan et al. [17] conducted many experiment to study the flame characteristics of heptane pool fires with different aspect ratios and orientations in a channel under the effect of sidewall effect, finally, an integral flame length model considering both sidewall effect and fuel shape is proposed. Sidewalls have been found to block air entrainment into the flame, leading to an increase in flame height [22–27]. Crosswise vortices drag the unburned fuel gas accumulated near the sidewall upward and transform the flame into longitudinal vortices as it interacts with the sidewall, resulting in a continuous increase in flame height [28]. However, with an increase in flame height, the thermal radiation feedback from the flame to a heptane pool fire surface was found to decrease because of the blockage of hot gases [29]. Recently, Zhang et al. [30, 31] conducted fire experiments with a rectangular fire source and a sidewall to examine the influence of the aspect ratio of the fire source on the flame morphology.

The flame split of a rectangular fire source with a high aspect ratio was observed using a digital charge-coupled device (CCD) camera [6] and a thermal infrared imager [12]. Compared with a square fire source, in a rectangular fire source with an aspect ratio larger than 4, the flame split into several split-flame branches. Furthermore, Hu et al. [32] reported the flame split of a square pool fire located at the near wake behind a square cylinder under horizontal wind flow. A recirculation zone with two shedding vortices was formed behind the cylinder. The flame was pulled by the vortices into two

opposite directions, which resulted in the flame split. However, for the fire scenarios without wind flow, the mechanism leading to the flame split of a rectangular fire source is unclear.

In the present study, the flame split of a rectangular fire source with a thin thermal sidewall was investigated using rectangular burners with equal surface areas but different aspect ratios placed against a steel plate. The flame morphology and temperature distribution on the back of the sidewall were measured. The mechanism for the flame branches following the flame split of a rectangular fire source with a high aspect ratio was analyzed. Finally, a physical model for flame split was developed, and the critical conditions for flame splitting were analyzed.

2. Experimental setup

Figure 1 shows a schematic of the experimental setup and burner shapes. The surface area of all burners was 900 cm^2, as in previous studies [6, 9, 12, 20]. However, the burners had different aspect ratios. A steady supply of propane controlled by a flow meter (measurement error: ±2%) served as the fuel supply. Table 1 lists the details of the fire scenarios. Each fire test was repeated twice to check the repeatability of the tests. Table 2 presents the thermal properties and dimensions of the steel plates used as sidewalls. A thin steel plate can be considered a thin thermal sidewall, with the temperature on the front side being equal to that on the back side. The temperature on the back side of the steel plate can be easily measured. Compared with an insulated board, the temperature on the back of the sidewall provides more information about a wall flame as well as the flame temperature. Furthermore, steel plates are commonly employed in building components [33], equipment [34], and concrete-filled steel-plate composite walls [35], and they can suffer damage during a fire.

No significant difference in flame temperature near the calcium silicate board and steel plate was found on the basis of experimental results of fire sources located against calcium steel plate and silicate board, which are not shown in this work. The flame buoyancy in the vertical direction

dominated the heat transfer between the flame and sidewall surface. The effect of the thermal properties of the sidewall on the flame temperature near the flame-exposed surface can be ignored.

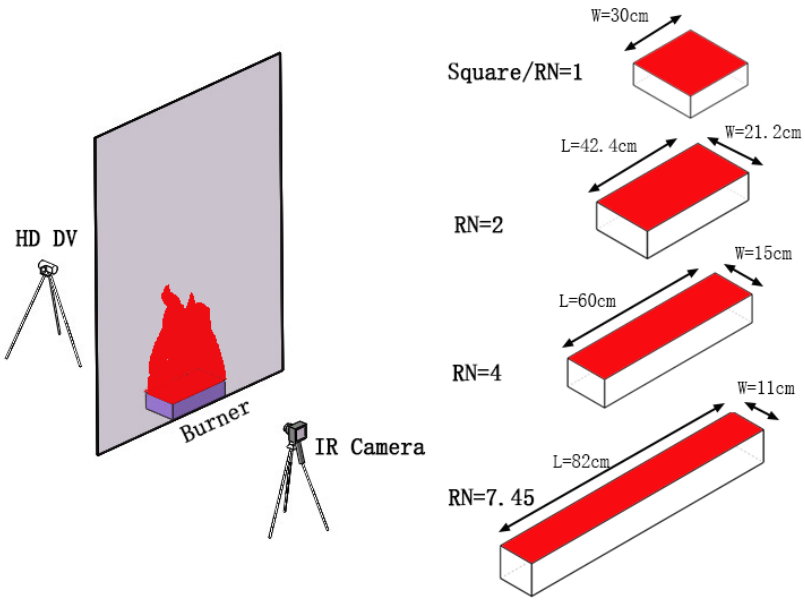

Fig. 1 Schematic of experimental setup.

Table 1 Summary of tested fire scenarios

Surface area (m^2)	Burner		Aspect ratio *RN*	Fire power $\dot{Q}$ (kW)
	Length (m)	Width (m)		
0.09	0.3	0.3	1	28.3; 42.4; 56.5; 70.7; 84.8
	0.424	0.212	2	
	0.6	0.15	4	
	0.82	0.11	7.4	

Table 2 Thermal physical properties of the steel plate

Material	Density (kg/m^3)	Conductivity (W/mK)	Sp. ht. cap. (kJ/kgK)	Length (m)	Width (m)	Thickness (m)
Steel	7860	68.4	0.46	2	1	0.0003

The flame shape was recorded using a digital CCD camera (resolution: 2592×1944 pixels) at 25 frames/s. Binary image processing technology was used to first calculate the flame height in the

binary image and then convert it into the real height [6]. An infrared camera (FLIR E85) was used to measure the temperature distribution on the back of the sidewall as shown in Fig. 1. From the images captured using the infrared camera, the temperature on the back side was obtained using FLIR TOOLs software version 5.13.17214.2001.

Thermocouple measurements were used to calibrate the measurement reliability of the infrared camera. The temperatures were measured using an array of 15 Type-K thermocouples having diameters of 0.5 mm, with error less than 0.75% and response time less than 1 s, placed at the centerline of the sidewall back side, as shown in Fig. 2. The first thermocouple was located 0.05 m above the burner surface. From the first thermocouple to the fifth, the thermocouples were spaced at 0.05-m intervals, whereas for those beyond the fifth, the distance between thermocouples was 0.1 m.

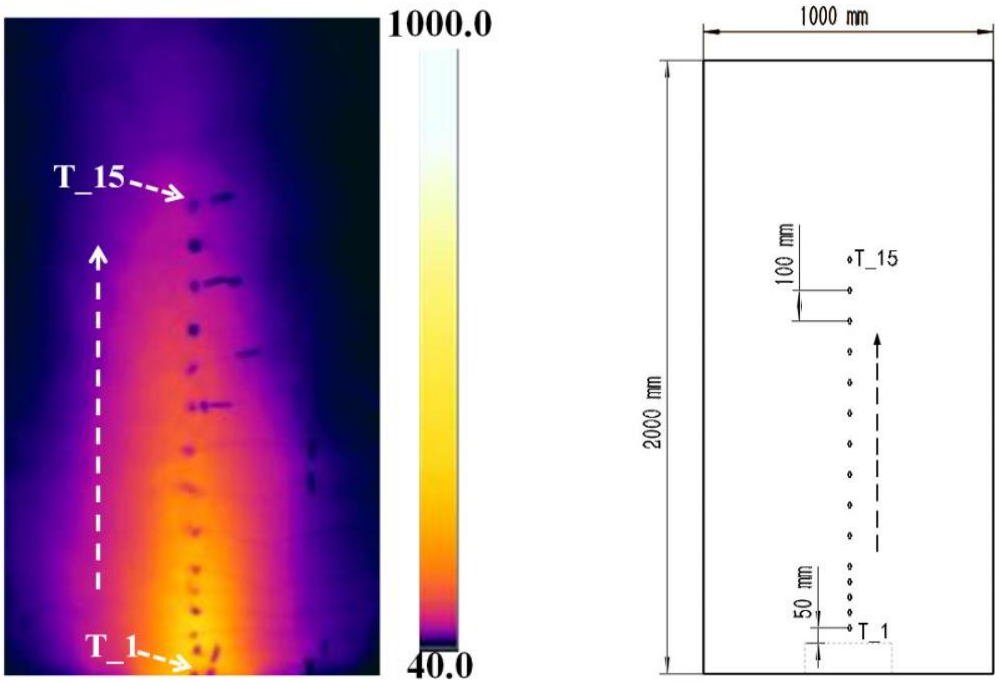

(a) (b)

Fig. 2 Distribution of the thermocouple points on the back side of the sidewall: (a) Image by the infrared camera, (b) Schematic of temperature measuring points.

Figure 3 shows the temperature evolution on the back side during the fire tests derived from the infrared camera images and thermocouples (RN = 1 and $\dot{Q}$ = 84.8 kW). The temperature values derived from the infrared camera were nearly the same as those measured by the thermocouples. Both temperatures reached a steady state approximately 100 s after the burner was ignited. In the analysis, the measurements of the thermocouples were set to standard, and the average error for the infrared camera was approximately 6.1%. This result validates the reliability of the experimental setup for the temperature distribution on the back side of the sidewall.

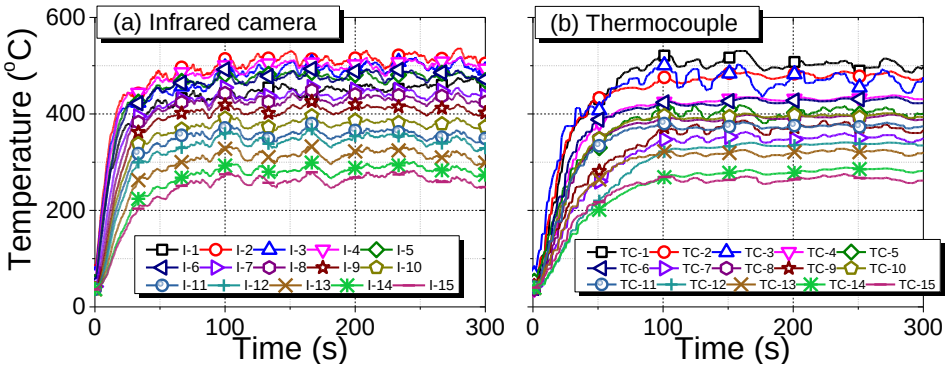

Fig. 3 Temperature evolution on the back side of the sidewall during the fire tests derived from the infrared camera images and thermocouples (RN = 1 and $\dot{Q}$ = 84.8 kW).

3. Experimental results and discussion

3.1 Flame morphology

Figure 4 shows the process of flame split with a 0.08-s time interval for the rectangular fire source with 7.45 aspect ratio and 84.8-kW heat release rate. A small hole appeared at the bottom and flame center in the beginning, as shown in Fig. 4(b). As the flame entrained the air and the flame height increased, the hole grew gradually larger, as shown in Fig. 4(c) – (f). At approximately 0.48 s, the flame from the rectangular fire source was split into two sub-flames, as shown in Fig. 4(g). Then, the sub-flames behaved separately and did not merge for a long time, at approximately 2.16 s.

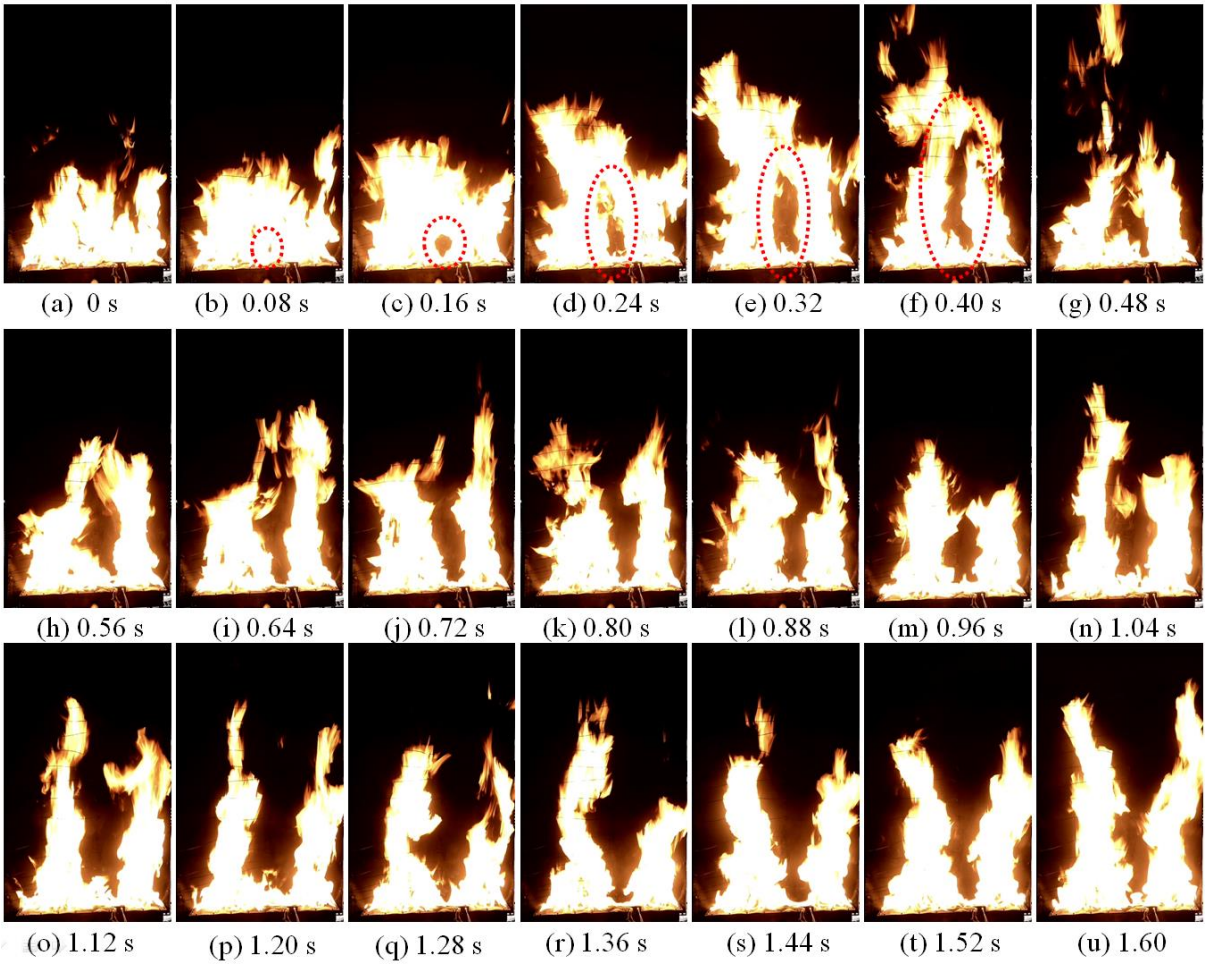

Fig. 4 Process of flame splitting with 0.08-s time interval (RN = 7.45, $\dot{Q}$ = 84.8 kW).

Figure 5 shows contour images of the flame-height frequency for rectangular fire sources of 84.8 kW with varying aspect ratios. When the aspect ratio was increased to 7.45, the flame split into two branches with a flame intermittency less than 0.7, as shown in Fig. 5(d). Figure 6 shows contour images of the flame-height frequency for rectangular fire sources having an aspect ratio of 7.45 and different heat release rates (HRRs). Except for the measurement at 84.8 kW, the complete flame region was divided into two branches for the burner with an aspect ratio of 7.45, and the average flame height of all split flame branches was almost the same.

Furthermore, the two split branches merged as the HRR increased, as shown in Figs. 5(d) and 6(f). The increase in the HRR led to higher flame buoyancy force in the vertical direction; the height of the small hole formed became higher. Furthermore, according to Eq. (3), with increasing HRR, the flame height became higher while the burner length was constant. Then, the ratio of the buoyancy force to the inertial force became greater. Subsequently, the two branches having intermittencies less than 0.7 merged.

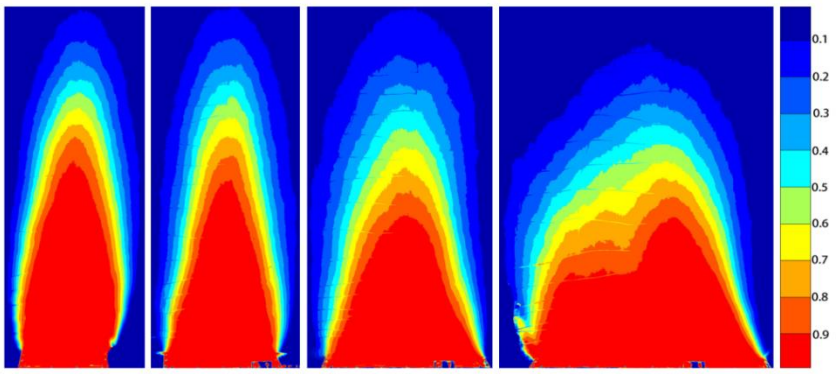

(a) (b) (c) (d)

Fig. 5 Contour images of the flame-height frequency for rectangular fire sources of 84.8 kW with varying aspect ratios: (a) *RN* = 1, (b) *RN* = 2, (c) *RN* = 4, (d) *RN* = 7.45.

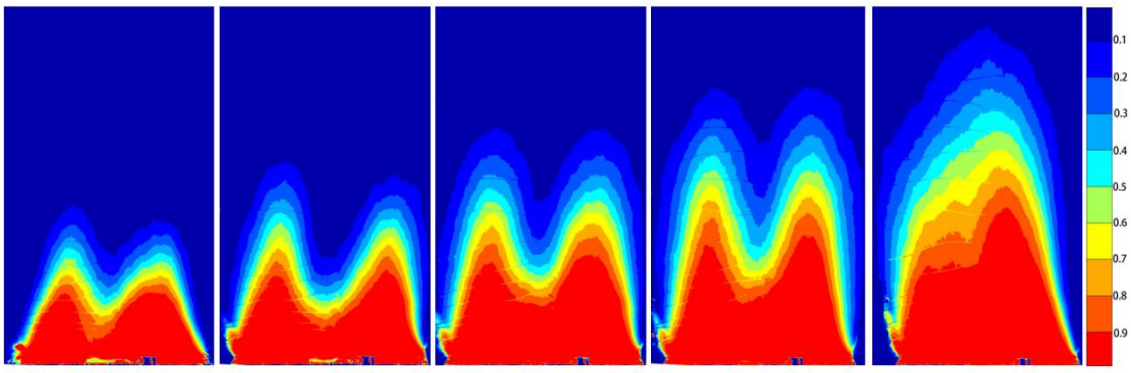

(a) (b) (c) (d) (e)

Fig. 6 Contour images of the flame-height frequency for rectangular fire sources having an aspect ratio of 7.45 and different HRRs: (a) 28.3 kW, (b) 42.4 kW, (c) 56.5 kW, (d) 70.7 kW, (e) 84.8 kW.

3.2 Temperature on the back of the sidewall

Figure 7 shows the temperature distribution on the back of the sidewall for rectangular fire sources at 84.8 kW with different aspect ratios. This temperature distribution was determined by the flame morphology. As the aspect ratio increased, the heated region on the sidewall decreased in the vertical direction and increased in the horizontal direction. This development corresponds to the effect of the aspect ratio on the flame morphology. For the burner with an aspect ratio of 7.45, the temperature distribution can be divided into two regions with HRR values from 28.3 kW to 84.8 kW. Furthermore, these two heated regions can be considered to be independent and heated by the two single flames, as shown in Fig. 8.

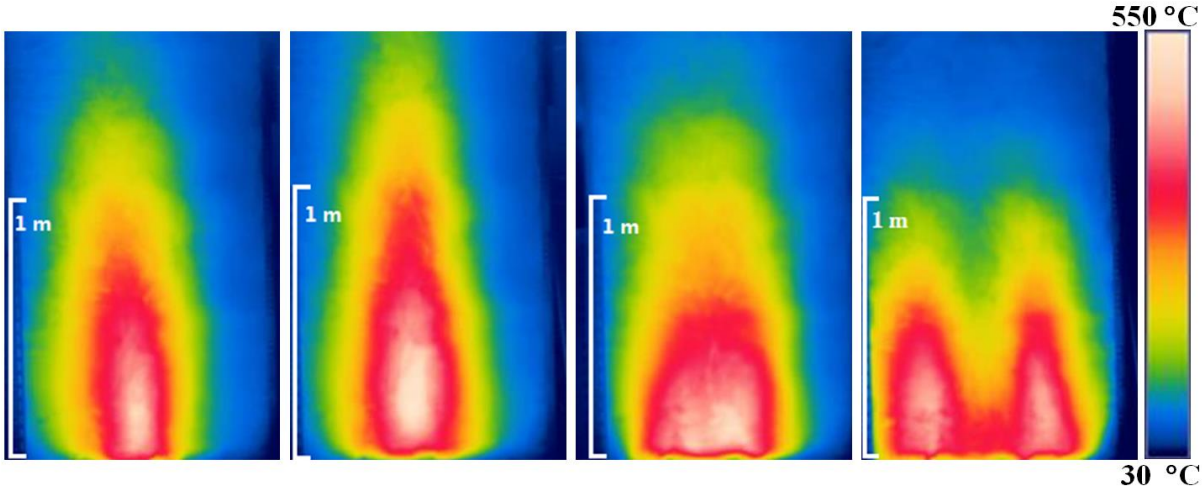

(a) (b) (c) (d)

Fig. 7 Temperature distribution on the back of the sidewall for rectangular fire sources at 84.8 kW with different aspect ratios: (a) *RN* = 1, (b) *RN* = 2, (c) *RN* = 4, (d) *RN* = 7.45.

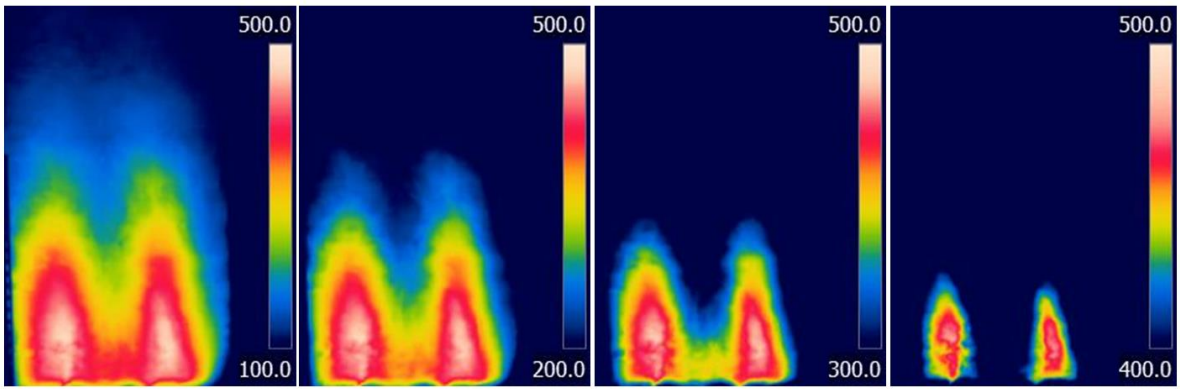

Fig. 8 Temperature distribution on the back of the sidewall with different temperature ranges (*RN* = 7.45, $\dot{Q}$ = 84.8 kW).

4. Numerical simulation and discussion

4.1 Model description

Large-eddy simulation (LES) has been previously used to simulate heat transfer from the flame to the sidewall [25, 36 – 38]. Livkiss et al. [38] used Fire Dynamics Simulator (FDS) version 6.7.0 [39] to study the fire-driven flow between two parallel vertical walls and a single vertical wall, which is similar to the fire scenarios reported in the present work. A Deardorff eddy viscosity model was used for the turbulent viscosity, and simple infinitely fast chemistry was used to model the turbulent combustion. The soot yield and radiative fraction of propane combustion were found to be 0.024 and 0.3, respectively. The number of radiation angles for the thermal radiation transfer was set to 300. The logarithmic-law convective heat transfer model was used for estimating convection between the flame and sidewall. Other parameters for simulation were set as default values in FDS, unless mentioned otherwise.

4.2 Numerical configurations

The computational domain for the fire scenarios was $2 \times 0.9 \times 2.2$ m^3 in the x, y, and z directions, respectively, as shown in Fig. 9. On the basis of mesh independent analysis, the predicted temperature

profiles by simulation with mesh sizes of 1 cm and 0.5 cm were almost coincident and close to the experimental data, as shown in Fig. 10. Therefore, a 1-cm mesh size was used in the simulation.

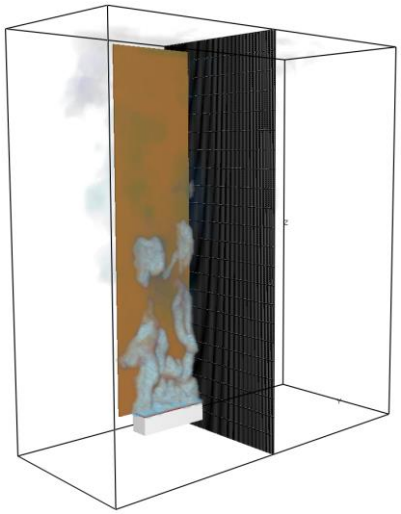

Fig. 9 Computational domain in the present work (RN = 7.45**,** $\dot{Q}$ = 84.8 kW).

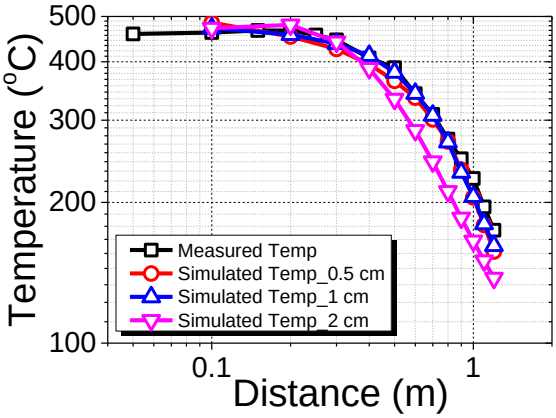

Fig. 10 Comparison between the measured and simulation temperature profiles of the sidewall back side with different mesh sizes (RN = 7.45, $\dot{Q}$ = 84.8 kW).

4.3 Simulated results and discussion

Figure 11 shows the flame morphology of the flame split process by numerical simulation. A hole was observed at the center of the flame. As the hole size increased, the flame was split into two sub-flames. Owing to the heat transfer from the flame to the sidewall, two heated zones were obtained on the sidewall back side for a burner with an aspect ratio of 7.45, as shown in Fig. 12. Simple infinitely fast chemistry was used for the simulation of the propane combustion. The approach assumes that the mixing of air and fuel is burnt. Therefore, a mixing zone of fuel and air was located at the fuel outlet. This mixing zone formed below where the flame was split. Then, a high-temperature zone was observed between the two heated zones. Generally, the simulation results conformed to the experimental results.

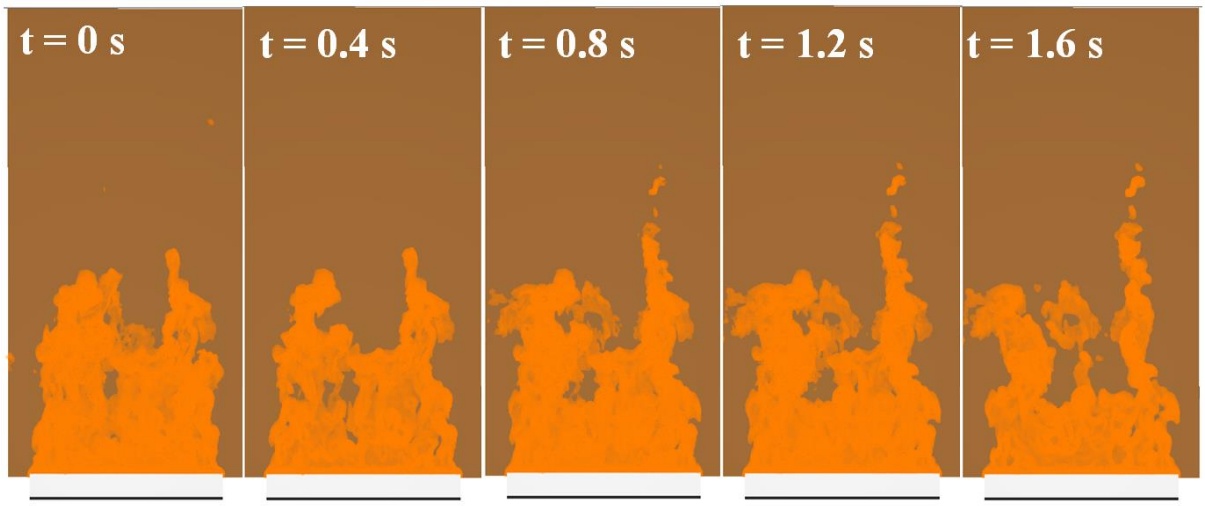

Fig. 11 Flame morphology of the flame split process by numerical simulation (RN = 7.45; $\dot{Q}$ = 84.8 kW).

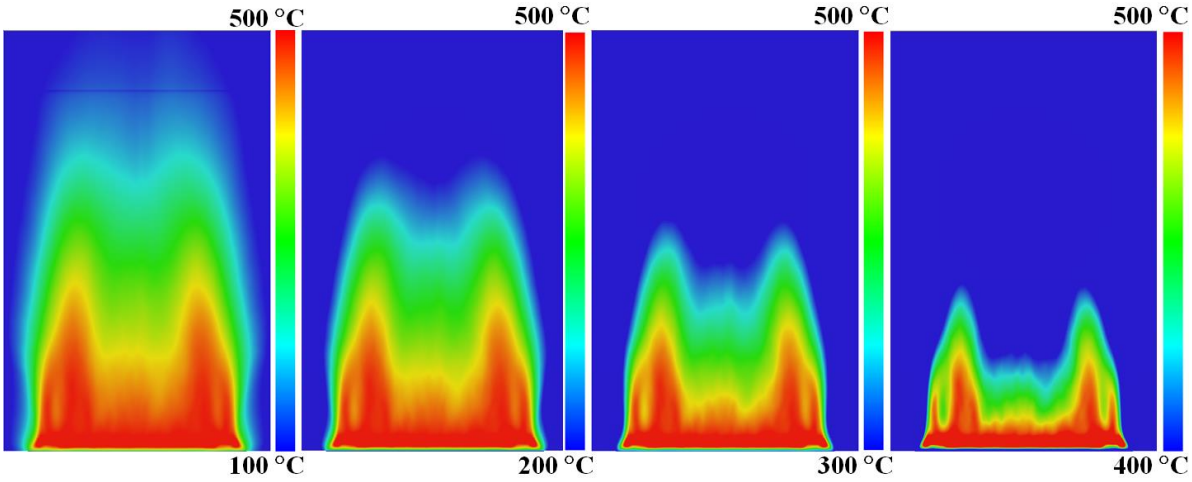

Fig. 12 Temperature distribution on the sidewall back side (*RN* = 7.45; $\dot{Q}$ = 84.8 kW).

Figure 13 shows the velocity vector and stream line of a cross section at 0.35 m from the fire source surface for the square and rectangular fire sources located against the sidewall. The entrained air from the middle of the length resulted in a flame split when the aspect ratio of the burner was 7.45. The upward velocity the fire plume facilitated the entrainment of air into the flame. Owing to the inertial force, the entrained air at the middle of the long side of the burner moved toward the sidewall. Concomitantly, the entrained air was consumed by combustion. The flame split occurred when the entrained air from the middle of the length was not consumed before it reached the bottom of the sidewall, as shown in Fig. 11(b). For the square burner, it was observed that the entrained air was consumed as it reached the center of the pool fire, as shown in Fig. 11(a). Crosswise flow stream formed near the sidewall. Subsequently, the air was entrained into the center of the pool fire. The crosswise vortices were transformed into longitudinal vortices. These simulated results are similar to those of the work by Jangi et al. [28]. This result proves the reliability of the simulation setup.

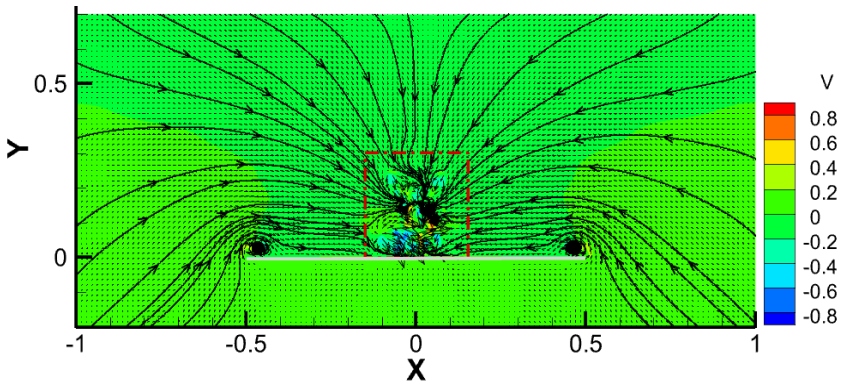

(a)

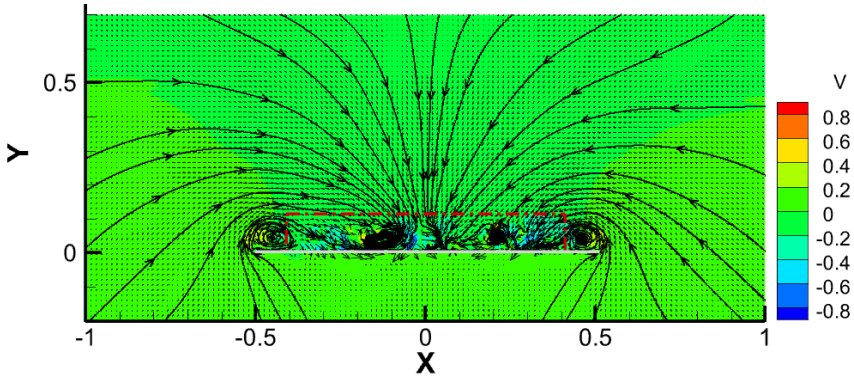

(b)

Fig. 13 Velocity vector and stream line of a cross section at 0.35 m from the fire source surface for the square and rectangular fire sources located against the sidewall: (a) RN = 1, $\dot{Q}$ = 28.3 kW; (b) RN = 7.45, $\dot{Q}$ = 28.3 kW.

5. Physical model for the flame split

Tan et al. [8] measured the velocity distribution of a flame on the horizontal section for a rectangular source fire. The experimental measurement revealed that the maximum vertical upward velocity $U_{m,z}$, was located at the centerline of the fire plume. Wan et al. [40] considered the horizontal air entrainment rate to be proportional to the vertical velocity at the centerline of the fire plume. Therefore, for a certain height less than the flame height, the horizontal air entrainment rate was at a maximum at the middle of the length of the rectangular burner, and it decayed along the long side to the end points, as shown in Fig. 14.

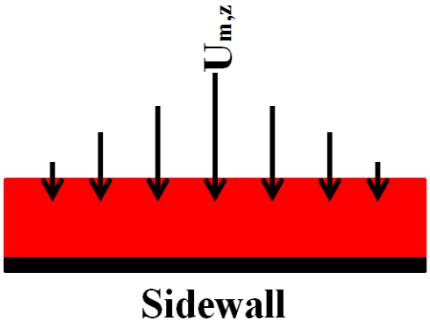

Fig. 14 Schematic of the horizontal air entrainment rate along the long side of a rectangular burner with sidewall.

The entrained air was transferred by the buoyancy force owing to the density difference and the inertial force caused by the Coandă effect to the side-entrained air flow on the flame-side surface [41]. This phenomenon resulted in the horizontal and vertical movement of the entrained air, as shown in Fig. 15.

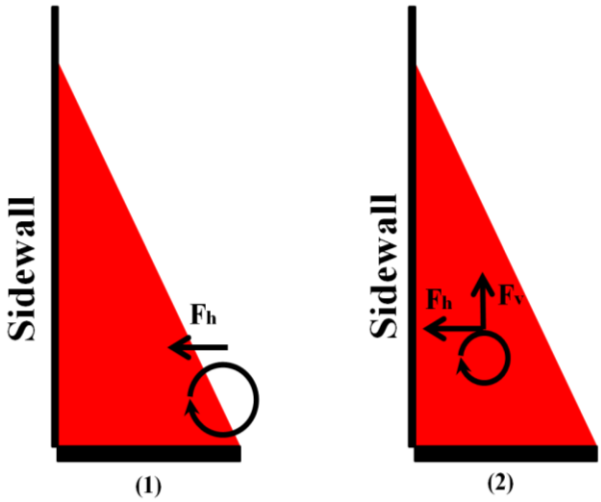

Fig. 15 Schematic of the movement of the entrained air in a rectangular flame source with a sidewall (side view).

The ratio of the buoyancy force to the inertial force exerted on the entrained air was used to determine the critical condition of the flame split. The flame buoyancy force in the vertical direction F_v can be expressed as [41]

$$F_v \sim \Delta\rho_f g L_f^3 \quad (1)$$

where $\Delta\rho_f$ is the density difference between ambient air and the flame, in kg/m^3; g is acceleration due to gravity, m/s^2; and L_f is the free flame height, m.

The inertial force in the horizontal direction F_h can be expressed as [41]

$$F_h \sim 0.5\rho_0 g L_f^2 L \quad (2)$$

where ρ_0 is the ambient air density, kg/m^3; and L is the fire source length, m.

Then, the ratio of the buoyancy force to the inertial force can be estimated as

$$F_v / F_h \sim L_f / L \quad (3)$$

Figure 16 shows the critical condition for the flame split of the source fire located against a sidewall. The ratio of the buoyancy force to the inertial force for the fire test in this work and that reported in the literature are listed in Table 3. The critical ratio of flame height to burner length for the flame split was approximately 0.9. In the fire experiments of the wall-attached flame conducted by Zhang et al. [19], the ratio of flame height to burner was greater than 2.0, and no flame split was observed. According to the observation in [29], as the ratio aspect increased, the flame can be roughly divided into three parts, which is similar to the flame morphology of the fire source with 7.45 aspect ratio and 84.8 kW.

The main objective of this work was to investigate the mechanism leading to the flame split. The rectangular fire source with aspect ratios 1, 2, 4, and 7.45 used in our previous work [6, 9, 12, 20] were selected in this work. A clear flame split was observed when the aspect ratio of the fire source was 7.45. As the aspect ratio decreased into 4, the flame splitting phenomenon disappeared. For the critical ratio of the buoyancy force to the inertial force for the fame split, more configurations are needed in future work.

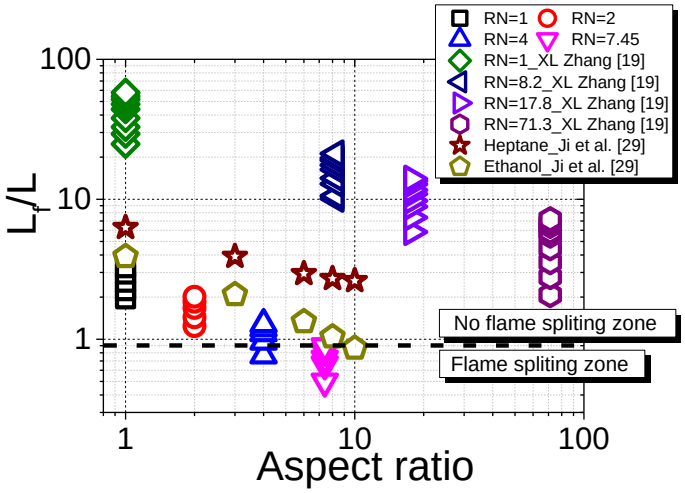

Fig. 16 Critical condition for the flame split of rectangular source fires.

Table 3 Ratio of the buoyancy force to the inertial force for fire test in this work and available in the literature

Fire tests in this work								**Heptane_Ji et al. [29]**	
Aspect ratio	L_f/L	Aspect ratio	L_f/L	Aspect ratio	L_f/L	Aspect ratio	L_f/L	Aspect ratio	L_f/L
1.00	1.95	2.00	1.24	4.00	0.77	7.40	0.50	1.00	6.27
1.00	2.22	2.00	1.43	4.00	0.96	7.40	0.66	3.00	3.91
1.00	2.55	2.00	1.68	4.00	1.11	7.40	0.73	6.00	2.94
1.00	2.92	2.00	1.85	4.00	1.20	7.40	0.82	8.00	2.71
1.00	3.24	2.00	2.01	4.00	1.28	7.40	0.89	10.00	2.62
XL Zhang et al. [19]								**Ethanol_Ji et al. [29]**	
Aspect ratio	L_f/L	Aspect ratio	L_f/L	Aspect ratio	L_f/L	Aspect ratio	L_f/L	Aspect ratio	L_f/L
1.00	24.82	8.25	10.09	17.81	5.84	71.25	2.07	1.00	3.90
1.00	29.32	8.25	10.60	17.81	7.41	71.25	2.79	3.00	2.09
1.00	32.82	8.25	12.88	17.81	8.86	71.25	3.56	6.00	1.33
1.00	37.97	8.25	14.14	17.81	9.77	71.25	4.48	8.00	1.04
1.00	44.02	8.25	16.29	17.81	10.92	71.25	5.50	10.00	0.86
1.00	47.81	8.25	17.57	17.81	11.65	71.25	5.88		
1.00	51.72	8.25	18.99	17.81	12.83	71.25	6.46		
1.00	54.38	8.25	19.64	17.81	13.54	71.25	6.76		
1.00	57.88	8.25	21.21	17.81	13.99	71.25	7.19		

6. Conclusions

The present study was conducted to investigate the flame split of a rectangular fire source with a sidewall. Rectangular fire sources with the same surface area but different aspect ratios were

considered. The burners were placed against a thermally thin steel plate. The temperature distribution on the back of the sidewall was measured to characterize the flame split. The flame split into two branches as the burner aspect ratio increased to 7.45, as evidenced by the two heated zones measured on the back of the sidewall.

A physical model was proposed to characterize the flame split for the fire source located against the sidewall. According to the numerical simulation results, the entrained air from the middle of the burner length led to the flame split as the aspect ratio of burner was 7.45. Then, the ratio of flame height to burner length for the flame split was proposed. According to the experimental data in the present work, the flame split can be observed for a ratio of flame height to burner length larger than 0.9. This critical ratio was validated by other fire experiments of fire sources against a sidewall reported in the literature. The developed physical model is applicable for fire sources located against a sidewall, and the effect of the distance between the flame and sidewall can be ignored.

Declarations of Interest: None

Acknowledgements:

This work was supported by the Guangdong Basic and Applied Basic Research Foundation (Grant No. 2021A1515012257), National Nature Science Funds of China (Grant No. 52076066), and the Guangzhou Science and Technology Plan Program of China (Grant No. 202002030124).

References

[1] Y Hasemi, M Nishihata. Fuel shape effect on the deterministic properties of turbulent diffusion flames, Fire Safety Sciences, 1987; 7:227-234.

[2] JG Qunitiere, BS Grove. A unified analysis for fire plumes, 27th Symposium on Combustion Institute, 1988; 2757-2766.

[3] LH Hu, XC Zhang, XL Zhang, et al. A re-examination of entrainment constant and an explicit model for flame heights of rectangular jet fires, Combustion and Flame, 2014;161:3000-3002.

[4] W Gao, NA Liu, Y Jiao, et al. Flame length of buoyant turbulent slot flame, Proceedings of the Combustion Institute, 2019; 3:3851-3858.

[5] ZH Zhou, GH Chen, CL Zhou, CL Zhou, Q Zhang. Experimental study on determination of flame height and lift-off distance of rectangular source fuel jet fires, Applied Thermal Engineering, 2019;152:430-436.

[6] XJ Huang, XJ Zhuo, T Huang, ZM Zheng, C Cheng, WK Chow. Simple flame height correlation for buoyancy-controlled diffusion plumes generated by rectangular sources fire with different aspect ratios, FUEL, 2019;254:115655.

[7] CZ Gong, L Ding, HX Wan, J Ji, ZH Gao, LX Yu. Spatial temperature n-heptane pool fires with different aspect ratios and heat fluxes received by adjacent horizontal targets, Fire Safety Journal, 2020;112:102959.

[8] TT Tan, L Ding, ZY Wang, J Ji, YQ Yang. Experimental study on the characteristics of buoyancy-driven turbulent flame generated by rectangular fire sources with different length-width ratios in an open space, FUEL, 2021;289:119778.

[9] XJ Huang, XJ Zhuo, T Huang, C Cheng, WK Chow. Thermal radiation model for the buoyancy-controlled diffusion plumes from rectangular fire sources, International Journal of Thermal Sciences, 2020; 15:106234.

[10] XC Zhang, LH Hu, W Zhu, et al. Axial temperature profile buoyant plume of rectangular source fuel jet fire in normal- and a sub- atmospheric pressure, FUEL,2014;15:455-459.

[11] LH Hu, F Tang, Q Wang, et al. Burning characteristics of conduction-controlled rectangular hydrocarbon pool fires in a reduced pressure atmosphere at high altitude in Tibet, FUEL, 2013;111:298-304.

[12] R Tu, J Fang, YM Zhang, et al. Effects of low air pressure on radiation-controlled rectangular ethanol and n-heptane pool fires, Proceedings of the Combustion Institute, 2013; 34:2591-2598.

[13] F Tang, LH Hu, ZW Qiu, et al. A global model of plume axial temperature profile transition from axisymmetric to line-source pool fires in normal and reduced pressures, Fuel, 2014;130:211-214.

[14] F Tang, KJ Zhu, MS Dong et al. Mean flame height and radiative heat flux characteristic of medium scale rectangular thermal buoyancy source with different aspect ratios in a sub-atmospheric pressure, International Journal of Heat and Mass Transfer, 2015;84:427-432.

[15] LH Hu, XC Zhang, XL Zhang, et al. Flame heights and fraction of stoichiometric air entrained for rectangular turbulent jet fires in a sub-atmospheric pressure, Proceedings of the Combustion Institute, 2017;36:2995-3002.

[16] CG Fan, JQ Zhang, KJ Zhu, KY Li. An experimental study of temperature and heat flux in a channel with an asymmetric thermal plume, Applied Thermal Engineering 2017; 113: 1128–1136.

[17] CG Fan, J Ji, YZ Li, H Ingason, JH Sun. Experimental study of sidewall effect on flame characteristics of heptane pool fires with different aspect ratios and orientations in a channel, Proceedings of the Combustion Institute, 2017; 36:3121-3129.

[18] Q Liu, CF Tao, Peng Wang, et al. The flame height of rectangular pool fires bounded by a sidewall with different distances and aspect ratios, Journal of Thermal Analysis and Calorimetry, 2019; 138:1415-1422.

[19] XL Zhang, LH Hu, MA Delichatsios et al. Experimental study on flame morphologic characteristics of wall attached non-premixed buoyancy driven turbulent flames, Applied Energy 2019;254:113672.

[20] XJ Huang, YH Wang, H Zhu, L He, F Tang, J Wen. Experimental study on the radiant heat flux of wall-attached fire plume generated by rectangular sources, International Jounral of Thermal Sciences, 2021;159:106605.

[21] XJ Huang, T Huang, X Zhuo, et al. A global model for flame pulsation frequency of buoyancy-controlled rectangular gas fuel fire with different boundaries, Fuel, 2021; 2:119857.

[22] EE Zukoski, T Kubota, B Cetegen et al. Entrainment in Fire Plumes, Fire Safety Journal. 1980/81; 3:107-121.

[23] Y Hasemi, T Tokunaga. Some Experimental Aspects of turbulent diffusion flames and buoyant plumes from fire sources against a wall and in a corner of walls, Combustion Science and Technology, 1984; 40:1-17.

[24] M Poreh, G Garrad. A study of wall and corner fire plumes, Fire Safety Journal, 2000; 34:1-98.

[25] F Tang, P Hu, Q He, JP Zhang, J Wen. Effect of sidewall on the flame extension characteristics beneath a ceiling induced by carriage fire in a channel, Combustion and Flame, 2021;223:202-215.

[26] ZS Li, YJ Gao, XS Li, PF Mao, YC Zhang, KY Jin, T Li, LF Chen. Effects of transverse fire locations on flame length and temperature distribution in a bifurcated tunnel fire, Tunneling and Underground Space Technology, 2021; 112:103893.

[27] ZX Tao, WJ Yang, ZH Sun, MZ Chen, J Wang, R Yang, H Zhang. Experimental study of oil pool shape and environment pressure on the wall fire behavior in an airplane cargo compartment, International Journal of Thermal Sciences, 2022;174:107440.

[28] M Jangi, BZ Dlugogorski. On wall fire fire interaction in a small pool fire: A large-eddy simulation study, Fire Safety Journal, 2017; 92:199-209.

[29] J Ji, TT Tan, ZH Gao, HX Wan. Influence of sidewall and aspect ratio on burning behavior of rectangular ethanol and heptane pool fires, Fuel, 2019; 238:166-172.

[30] XL Zhang, LH Hu, MA Delichatsios et al. Experimental study on flame morphologic characteristics of wall attached non-premixed buoyancy driven turbulent flames, Applied Energy, 2019:254:113672.

[31] XL Zhang, X Fang, LH Hu. Buoyant turbulent diffusion flame heights of free-, wall- and corner air entrainment conditions: Experiments and global model based on mirror approach, FUEL, 2021; 303:121338.

[32] LH Hu, XY Zhao, W Zhu, et al. An experimental investigation and characterization on flame bifurcation and leaning transition behavior of a pool fire in near wake of square cylinder, International Journal of Heat and Mass Transfer, 2021;55:7024-7035.

[33] D Kamikawa, Y Hasemi, T Wakamatsu, et al. Experimental flame heat transfer correlations for a steel column adjacent to and surrounded by a pool fire, Fire Safety Science. 2003;7: 989-1000.

[34] J Siva, A Landesmann, F Ribeiro. Performance-based analysis of cylindrical steel containment vessels exposed to fire, Fire Safety Journal. 2014; 69:126-135.

[35] F Wei, C Fang, B Wu. Fire resistance of concrete-filled steel plate composite (CFSPC) walls, Fire Safety Journal. 2017; 88:26-39.

[36] N Ren, Y Wang, Sébastien Vilfayeau et al. Large eddy simulation of turbulent vertical wall fires supplied with gaseous fuel through porous burners, Combustion and Flame, 2016;169:194-208.

[37] N Ren, Y Wang. A convective heat transfer model for LES fire modeling, Proceedings of the Combustion Institute, 2021:28:4535-4542.

[38] K Livkiss, BP Husted, T Beji et al. Numerical study of a fire-driven flow in a narrow cavity, Fire Safety Journal, 2019;108:102834.

[39] K. McGrattan, S. Hostikka, R. McDermott, J. Floyd, M. Vanella, Fire Dynamics Simulator User's Guide, Sixth Edit, 2018.

[40] HX Wan, J Ji, KY Li, XY Huang, JH Sun, YM Zhang. Effect of air entrainment on the height of buoyant turbulent diffusion flames for two fires in open space, Proceedings of the Combustion Institute, 2017: 36: 3003-3010.

[41] XL Zhang, LH Hu, XC Zhang, et al. Experimental investigation and analysis of flame height transition and air entrainment of near-wall rectangular-source fires at various distances, Proceedings of the Combustion Institute, 2020;19:15-32.